

**Supplementary Informations**  
**Quantum Interferences and**  
**Electron Transfer in Photosystem I**

Nicolas Renaud,\* Daniel Powell, Mahdi Zarea, Bijan Movaghar, Michael R.  
Wasielewski, and Mark A. Ratner

*Northwestern University, Department of Chemistry 2145 Sheridan Road, Evanston, IL,  
60208-3113*

E-mail: n-renaud@northwestern.edu

---

\*To whom correspondence should be addressed

# The Stochastic Surrogate Hamiltonian

The SSH approach proposes to simulate the dynamics of a system of interest in interaction with a bath. The bath is a priori constituted of an infinite number of modes but to reduce the numerical cost only a few number of representing modes are considered. The Hamiltonian of this bath is hence:

$$\mathcal{H}_B = \sum_{q=1}^Q \omega_q \sigma_q \sigma_q^\dagger \quad (1)$$

where  $\omega_q$  is the frequency of the  $q$ -th bath modes with  $\sigma_q^\dagger$  ( $\sigma_q$ ) its creation (annihilation) operator. The frequency of these modes is randomly chosen according to the bath spectral density. For the super-Ohmic spectral density considered here, these frequencies are chosen from a Gaussian distributed random generator whose parameters has been chosen to fit correctly the bath spectral density as represented in Fig. 3b. The cutoff frequency of this Gaussian was set to 150 meV and its width to 50 meV. This random sampling slightly overestimate(underestimate) the number of bath modes at low(high) frequency but is a major improvement compared to a uniform random distribution of the bath modes. The interaction between the system and the bath are defined to simulate electronic quenching between state of different energy and reads:

$$\mathcal{H}_{SB} = \mathcal{R}_S \otimes \sum_{q=1}^Q \lambda_q (\sigma_q^\dagger + \sigma_q) \quad (2)$$

where  $\mathcal{R}_S$  defines the relaxation pathways within the system of interest and  $\lambda_q$  the interaction strength between the states of the system and the bath modes. The diagonal elements of  $\mathcal{R}_S$  represent uncorrelated modes that only acts on a given site. At the contrary the off diagonal elements of the  $\mathcal{R}_S$  model correlated modes that enable the electronic density to go from site  $n$  to site  $m$  by emitting a phonon in the bath.

Quantum jumps were performed during the temporal evolution of the electronic density. Each quantum jump reset a specific bath modes to its thermal state removing energy from the total

system. To perform these quantum jumps a jump rate is defined for each mode following:

$$\Gamma_q = \Lambda \times \lambda_q \quad (3)$$

The ration  $\Lambda$  controls the jump rate of every one. For large value of  $\Lambda$  the bath modes are constantly reset to their thermal state and for small values of  $\Lambda$  the bath modes are more likely to give energy back into the system. Hence  $\Lambda$  defines the degree of Markovianity of the propagation scheme. To remain in the Markovian limit,  $\Lambda$  is set to  $\Lambda = 1.05 \text{ eV}^{-1} \text{ fs}^{-1}$  which gives a life time of the bath of  $\Gamma_q \simeq 10 \text{ fs}$  for the strongly interacting modes. For each mode the jump condition is fixed by:

$$\exp(-\Gamma_q \tilde{t}_q) < \varepsilon_q \quad (4)$$

where  $\tilde{t}_q$  is the time elapsed since the last jump on mode  $q$  and  $\varepsilon_q$  a random number ranging between 0 and 1 and reset after each jump on mode  $q$ . For each time step, if the condition (4) is met then the bath mode  $q$  is reset. The jump procedure require the computation of the partial trace of the total density matrix to access rigorously the state system and the state of each mode. Hence to perform a jump the reduced density matrix (RDM) of the system ( $\rho_S(t)$ ), the RDM of the bath ( $\rho_B(t)$ ) and the RDM of each bath modes ( $\rho_{b_n}(t)$ ) are computed via:

$$\rho_S(t) = Tr_B[\rho(t)] \quad \rho_B(t) = Tr_S[\rho(t)] \quad \rho_{b_n}(t) = Tr_{i \neq n}[\rho_B(t)] \quad (5)$$

A jump on the  $k$ -th mode is then performed by replacing the its RMD by its thermal RDM:

$$\rho_{b_k}(t) \leftarrow \frac{1}{2 \cosh(2\Omega_k)} \begin{pmatrix} e^{-\Omega_k} & e^{-i\theta} \\ e^{i\theta} & e^{\Omega_k} \end{pmatrix} \quad (6)$$

with:  $\Omega_k = \frac{\hbar\omega_k}{2k_bT}$ ;  $\theta$  a random phase factor;  $T$  the temperature of the bath. The total density matrix is then recomputed following:

$$\rho(t) = \rho_S(t) \otimes \rho_{b_1}(t) \otimes \dots \otimes \rho_{b_Q}(t) \quad (7)$$

and the propagation can continue on the next step. This expansive numerical procedure allows to perform rigorously a jump on a given bath modes and destroys coherence within the system. Since only a time-independent Hamiltonian was studied here, the coherent propagation between  $t$  and  $t + \Delta t$  is operated by the evolution operator following:

$$\rho(t + \Delta t) = e^{-i\mathcal{H}\Delta t} \rho(t) e^{i\mathcal{H}\Delta t} \quad (8)$$

Due to the statistical approach employed by the SSH to sample the bath density and the stochastic quantum jumps, the Liouville equation must be solved several times to converge toward the final dynamics. The initial condition of the Liouville equation is supposed to be a non-entangled superposition of an excited state of the principal system and the thermal state of the bath:  $\rho(0) = \rho_S(0) \otimes_{q=1}^Q \rho_q^T$  supposing that the excitation of the system destroys any system/bath entanglement.

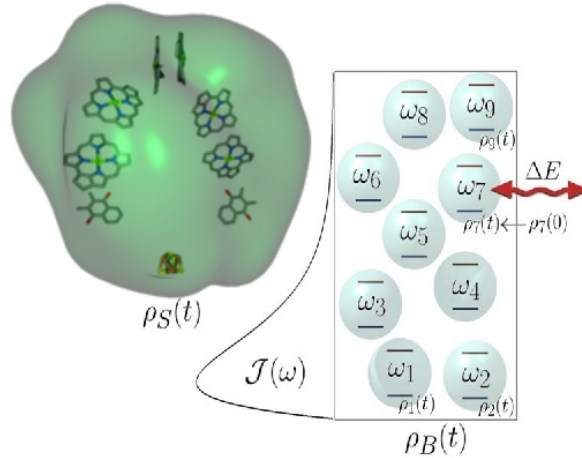


Figure 1: Graphical representation of the isolated PSI ETC in interaction with the bath modes modeling its environment. Only Few bath modes are explicitly treated and quantum jumps are performed on the bath manifold.

## Electronic Structure and on-site energies

Electronic structure calculations were performed on the different fragment composing the PSI using a standard DFT approach using B3LYP functional and a DZ basis set. These calculations were performed on the relaxed geometry of each fragment after the removal of the carotene tail. These calculations were performed both in gas phase and using a solvent of dielectric  $\epsilon = 4$ . The results of these calculations for the organic fragments is presented in Fig. 2. In this figure is represented the LUMO of each fragment and its ionization potential (IP) and electron affinity (EA) both in gas phase and in solvent. Our calculations were unable to provide accurate results for the electronic structure of the iron-sulfur cluster. Hence the experimental value of its on-site energy was adopted in our model.

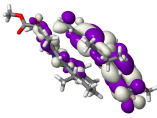
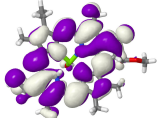
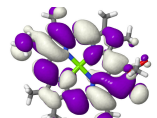
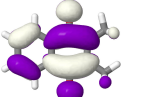
Special Pair		Chl-A <sub>0</sub>	
	EA (GP)	1.42 eV	
	EA ( $\epsilon = 4$ )	2.10 eV	
	IP (GP)	5.43 eV	
	IP ( $\epsilon = 4$ )	4.38 eV	
Chl-A		PhQ	
	EA (GP)	1.33 eV	
	EA ( $\epsilon = 4$ )	2.25 eV	
	IP (GP)	6.23 eV	
	IP ( $\epsilon = 4$ )	5.61 eV	
		EA (GP)	1.08 eV
		EA ( $\epsilon = 4$ )	2.97 eV
		IP (GP)	8.70 eV
		IP ( $\epsilon = 4$ )	7.66 eV

Figure 2: Electronic structure of the special pair, Chl-A, Chl-A<sub>0</sub> and PhQ. The Electron Affinity (EA) and ionization potential (IP) are reported for a gas phase and a dielectric solvent

On top of these intrinsic parameters the Coulombic attraction between the propagating electron and the hole remaining at the special pair was accounted for with a simple point charge approximation. More advanced calculations are possible but this simple approximation is supposed to be good enough and is not thought as the principal source of error in our model. The value of the

electrostatic force are reported in the table below.

$E_c(P700^+/Chl - A^-)$	0.34 eV	@ 0.72 nm
$E_c(P700^+/Chl - A_0^-)$	0.16 eV	@ 1.51 nm
$E_c(P700^+/PhQ^-)$	0.10 eV	@ 2.31 nm
$E_c(P700^+/Fx^-)$	0.08 eV	@ 3.10 nm

Now that all the EA and IP and electrostatic interactions are calculated, we can compute the on-site energy of each fragments following :

$$E_X = IP_{P700} - E_{hv} - EA_X + E_c(P700^+/X^-) \quad (9)$$

The results of these calculations are given below:

Chl-A <sub>0</sub>	$E_{Chl-A} \simeq 4.38 - 1.77 - 2.25 - 0.35 = 0.005$ eV
Chl-A	$E_{Chl-A_0} \simeq 4.38 - 1.77 - 2.46 - 0.16 = -0.011$ eV
PhQ	$E_{PhQ} \simeq 4.38 - 1.77 - 2.97 - 0.10 = -0.460$ eV

## Charge Transfer Integral

The charge transfer integrals were computed directly via the spatial overlap of LUMO of each fragments giving a much better approximation than the split orbital method. These calculations were performed using the optimized geometry of each dimer and are reported in Fig. 1. A large coupling was obtained between the two state of the special pair due to their close proximity. The two Chl of each branch also strongly interact and all the other coupling are much weaker. The signs of the coupling are due to the relative orientation of the LUMO of each fragment. Each  $\pi_z$  orbital carry a positive and negative phase on each lobe and the overlap between two  $\pi_z$  is sensitive to this phase. Hence depending on the orientation/delocalisation of each molecular orbital the overall coupling can either be positive or negative. This sign influence the phase of the wave function during its propagation between two sites but not its magnitude. However, the interference strongly depends on this phase.

## Relaxation matrix

In the interaction Hamiltonian the electron-phonon interaction are given by:  $\lambda_q = \frac{1}{\sqrt{Q}} \mathcal{J}(\omega_q)$ . Depending on the matrix element of  $\mathcal{H}_S$  different mechanism can be simulated. In a more classical way the interaction Hamiltonian can be written as:

$$\mathcal{H}_{SB} = \sum_{n=1}^N \sum_{m=1}^N \sum_{q=1}^Q \frac{r_{nm}}{\sqrt{Q}} \mathcal{J}(\omega_q) |s_n\rangle \langle s_m| (\sigma_q^\dagger + \sigma_q) \quad (10)$$

The diagonal elements  $r_{nn}$  introduce dephasing but not energy relaxation. On the contrary the off-diagonal element simulate phonon-assisted transition where the electronic density can transfer from  $|n\rangle$  to  $|m\rangle$  by emitting a phonon in the bath. To account for the spatial dependence of this transition the  $r_{nm}$  are computed via the overlap of two identical Gaussian centered on state  $n$  and  $m$  as represented in Fig. 3a. This overlap reads:

$$r_{nm} = \int_{-\infty}^{\infty} d^3r \frac{\beta}{\sqrt{\pi}} e^{-\beta^2 r^2} e^{-\beta^2 (r-d_{nm})^2} = e^{-3/4\beta^2 d_{nm}^2} \quad (11)$$

With the center to center distances obtained via the X-ray structure of PSI the values of the  $r_{nm}$  matrix elements reported in Fig. 3a were obtained and used in the simulations.

## Bath Spectral density

To model the bath spectral density used a super-ohmic density of states is used:

$$\mathcal{J}(\omega) = \lambda (\omega/\omega_c)^2 e^{-(\omega/\omega_c)^2} \quad (12)$$

To fit the vibrations modes of the fragments constituting PSI, we set:  $\omega_c = 0.15$  eV and  $\lambda = 50$  meV leading to the spectral distribution represented in Fig. 3b. This spectral density account correctly for most of the vibration modes of the Chl's and PhQ's but completely neglect the C-H stretch modes located around 0.5 eV.

Using a super-ohmic spectral density allows to sample accurately the bath spectral density. Hence the value of the frequencies,  $\omega_q$ , are randomly set using a Gaussian distributed random number generators implemented in the GNU Scientific Library. The Gaussian distribution used during our calculations to set the values of the  $\omega_q$  is represented in Fig, 3b and is very similar to the actual bath spectral density,  $\mathcal{J}(\omega)$ .

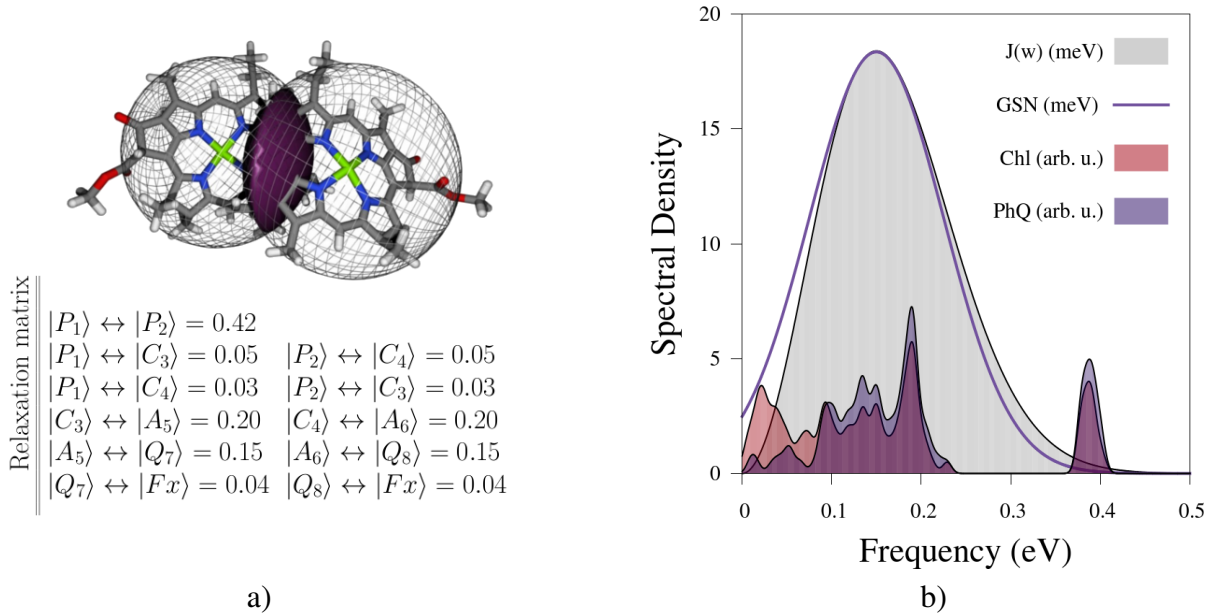


Figure 3: a) Representation of the method employed to compute the matrix elements of  $\mathcal{R}_S$  which are defined by the spatial overlap between two Gaussian centers on the two fragments. b) Bath spectral density defined in super-ohmic density, Gaussian random distribution and vibration frequencies of the Chl's and PhQ's

## Destructive Interference: block diagonalisation

To understand the origin of the quantum interference, a block diagonalisation of the Hamiltonian  $\mathcal{H}_S$ , on the subspace  $\{|P_1\rangle, |P_2\rangle\}$  is useful. This block diagonalisation is obtained by:  $\tilde{\mathcal{H}}_S = R(\pi/2)\mathcal{H}R^\dagger(\pi/2)$  where  $R(\pi/2)$  is a rotation matrix on the  $\{|P_1\rangle, |P_2\rangle\}$  subspace. Doing so one obtain:

$$\tilde{\mathcal{H}}_S = \begin{pmatrix} |\Psi^-\rangle & |\Psi^+\rangle & |C_3\rangle & |C_4\rangle & |A_5\rangle & |A_6\rangle & |Q_7\rangle & |Q_8\rangle & |Fx\rangle \\ -6.9 & 0 & -4.2 & 4.2 & . & . & . & . & . \\ 0 & 6.9 & 1.4 & 1.4 & . & . & . & . & . \\ -4.2 & 4.2 & 5 & . & -4.0 & . & . & . & . \\ 1.4 & 1.4 & . & 5 & . & -4.0 & . & . & . \\ . & . & -4.0 & . & -11 & . & -0.1 & . & . \\ . & . & . & -4.0 & . & -11 & . & -0.1 & . \\ . & . & . & . & -0.1 & . & -460 & . & 0.01 \\ . & . & . & . & . & -0.1 & . & -460 & 0.01 \\ . & . & . & . & . & . & 0.01 & 0.01 & -700 \end{pmatrix} \quad (13)$$

where  $|\Psi^+\rangle$  and  $|\Psi^-\rangle$  are the two initial state considered in the Fig. 2 and 3 respectively. The large oscillation obtained in Fig 2 where starting from  $|\Psi^+\rangle$  are due to the near resonance between  $|\Psi^+\rangle$  and  $|C_3\rangle$  and  $|C_4\rangle$ . The direct coupling between these two states leads to the Rabi-like oscillations observed in Fig. 2. When starting from  $|\Psi^-\rangle$  one obtain fast oscillations on  $|A_5\rangle$  and  $|A_6\rangle$  since they are close in energy from the initial state. However as explain in the text  $|\Psi^-\rangle$  interacts with a positive and negative coupling with  $|C_3\rangle$  and  $|C_4\rangle$  respectively. This sign inversion in the coupling of the initial state with the two branch is responsible of the quantum interference observed on the electronic density dynamics. These interference can be explained as  $\pi$  phase difference between the components of the wave function that propagates one each branch. Half of the wave function evolves along the right branch and the other half evolves on the other branch but with an opposite phase. Hence when they recombine on the cluster they cancel each other, and the wave function never reaches Fx. Another way of looking at this interference is based on the diagonalization of the Hamiltonian and is presented in the next section for a 4-level system.

## Destructive Interference in a 4-level systems

A classic example of destructive interference is observed in a four level system whose Hamiltonian reads:

$$\mathcal{H}_0 = \begin{matrix} & \begin{matrix} |\phi_1\rangle & |\phi_2\rangle & |\phi_3\rangle & |\phi_4\rangle \end{matrix} \\ \begin{pmatrix} E & -\alpha & \alpha & . \\ -\alpha & E & . & \alpha \\ \alpha & . & E & \alpha \\ . & \alpha & \alpha & E \end{pmatrix} & \end{matrix} \quad (14)$$

Starting from  $|\phi_1\rangle$ , the evolution of this system given by:  $|\Psi(t)\rangle = e^{-i\mathcal{H}_0 t}|\phi_1\rangle$  never reaches  $|\phi_4\rangle$  due to similar quantum interference which is characterized by:  $P_f = |\langle\phi_4|\Psi(t)\rangle|^2 = 0$ . To understand the origin of these destructive interference one can write the diagonalisation matrix of  $\mathcal{H}_0$ :

$$\mathbf{U} = \begin{matrix} & \begin{matrix} |\Psi_1\rangle & |\Psi_2\rangle & |\Psi_3\rangle & |\Psi_4\rangle \end{matrix} \\ \begin{pmatrix} 0 & -1/\sqrt{2} & -1/\sqrt{2} & 0 \\ -1/2 & 1/2 & -1/2 & 1/2 \\ -1/2 & -1/2 & 1/2 & 1/2 \\ 1/\sqrt{2} & 0 & 0 & 1/\sqrt{2} \end{pmatrix} & \begin{matrix} \langle\phi_1| \\ \langle\phi_2| \\ \langle\phi_3| \\ \langle\phi_4| \end{matrix} \end{matrix} \quad (15)$$

where  $|\Psi\rangle$  are the eigenstates of Hamiltonian (14). The initial state  $|\phi_1\rangle$  and the target state  $|\phi_4\rangle$  belong to orthogonal subspace. The evolution of the system on the eigenbasis reads:

$$|\Psi(t)\rangle = \frac{-1}{\sqrt{2}}(e^{-i\lambda t}|\Psi_2\rangle + e^{i\lambda t}|\Psi_3\rangle) \quad (16)$$

where  $\lambda = E + \sqrt{2}\alpha$ . Projecting on  $\langle\phi_4|$  leads to:

$$\langle \phi_4 | \Psi(t) \rangle = \frac{1}{2} (\langle \Psi_1 | + \langle \Psi_4 |) (e^{-i\lambda_2 t} | \Psi_2 \rangle - e^{-i\lambda_3 t} | \Psi_3 \rangle) = 0 \quad (17)$$

As we just simply demonstrated the evolution starting from  $|\phi_1\rangle$  never reaches  $|\phi_4\rangle$  because these two states belong to orthogonal subspaces. Another way to demonstrate these destructive interference is to compute the projection of  $|\Psi(t)\rangle$  on the middle states  $|\phi_2\rangle$  and  $|\phi_3\rangle$ :

$$\langle \phi_2 | \Psi(t) \rangle = \frac{-1}{2\sqrt{2}} (e^{-i\lambda t} - e^{i\lambda t}) = 1/\sqrt{2} \sin(\lambda t + \pi) \quad (18)$$

$$\langle \phi_3 | \Psi(t) \rangle = \frac{1}{2\sqrt{2}} (e^{-i\lambda t} - e^{i\lambda t}) = 1/\sqrt{2} \sin(\lambda t) \quad (19)$$

The two component evolves with opposite phase which ultimately leads to the destructive interference much like in an optical interferometer.

## Effect of the detuning

The biphasic rate observed for a large value of the detuning can be simply explained in terms of incoming and out-coming rate to and from the PhQ. For the sake of the demonstration we consider a positive detuning where the energy of  $|Q_8\rangle$  is lowered down by 0.15 eV. Reducing the on-site energy of  $|Q_8\rangle$ , leads to a large energy difference between  $|A_6\rangle$  and  $|Q_8\rangle$ . Few bath modes are then available to assist the electronic density in hopping from this Chl-A<sub>0</sub> to the PhQ which gives a slow incoming rate on  $|Q_8\rangle$ . Similarly, the energy difference between  $|Q_8\rangle$  and  $|Fx\rangle$  is reduced when decreasing the on-site energy of  $|Q_8\rangle$ . More bath modes are then available to assist the transfer of the electronic density from the PhQ to the cluster. Consequently the rate of this transfer is increased by the detuning. As a consequence the accumulation of the electronic density on  $|Q_8\rangle$  is decreased since the injection of the electronic density on this state becomes much slower than the transfer rate from  $|Q_8\rangle$  to the iron-sulfur cluster.

We have observed an enhancement of the quantum yield for a detuning of 0.15 eV with the initial condition  $|\Psi^-(0)\rangle$ . This enhancement is also observed for different initial state. Fig. 4 represent the variations of the quantum yield with the amplitude of the random fluctuations and the value of the detuning for the initial state  $|\Psi^-(0)\rangle$  (left) and  $|\Psi^+(0)\rangle$  (right). The random fluctuations suppress the effect of the constructive or destructive interference. However for both initial condition a maximum quantum yield is observed for a detuning of  $\Delta E = 0.15$ .

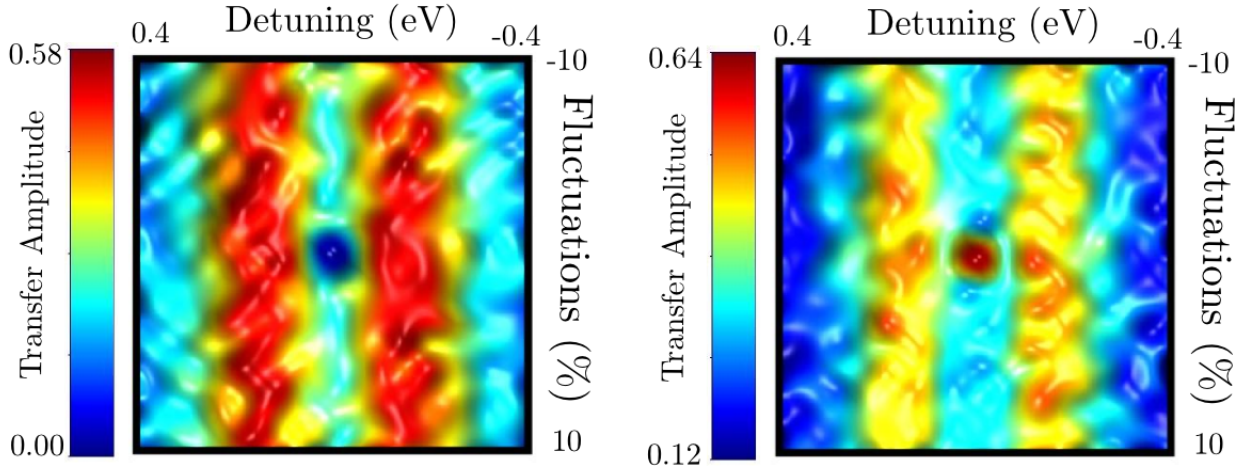


Figure 4: Variations of the quantum yield with the amplitude of the random fluctuations and the value of the detuning for the initial state  $|\Psi^-(0)\rangle$  (left) and  $|\Psi^+(0)\rangle$  (right)